Stimulation of a Suprachoroidal Retinal Prosthesis Drives Cortical Responses in a Feline Model of Retinal Degeneration

Felix P. Aplin,[1–3] Erica L. Fletcher,[2] Chi D. Luu,[1,4] Kirstan A. Vessey,[2] Penelope J. Allen,[1] Robyn H. Guymer,[1,4] Robert K. Shepherd,[3,5] and Mohit N. Shivdasani[3,5]

[1]Centre for Eye Research Australia, Royal Victorian Eye and Ear Hospital, East Melbourne, Victoria, Australia
[2]Department of Anatomy and Neuroscience, The University of Melbourne, Melbourne, Victoria, Australia
[3]The Bionics Institute, East Melbourne, Victoria, Australia
[4]Department of Surgery (Ophthalmology), The University of Melbourne, Parkville, Victoria, Australia
[5]Medical Bionics Department, The University of Melbourne, Melbourne, Victoria, Australia

Correspondence: Erica L. Fletcher, Department of Anatomy and Neuroscience, University of Melbourne, Victoria, 3010, Australia; elf@unimelb.edu.au.

Submitted: May 13, 2016
Accepted: August 8, 2016

Citation: Aplin FP, Fletcher EL, Luu CD, et al. Stimulation of a suprachoroidal retinal prosthesis drives cortical responses in a feline model of retinal degeneration. *Invest Ophthalmol Vis Sci*. 2016;57:5216–5229. DOI:10.1167/iovs.16-19926

Purpose. Retinal prostheses have emerged as a promising technology to restore vision in patients with severe photoreceptor degeneration. To better understand how neural degeneration affects the efficacy of electronic implants, we investigated the function of a suprachoroidal retinal implant in a feline model.

Methods. Unilateral retinal degeneration was induced in four adult felines by intravitreal injection of adenosine triphosphate (ATP). Twelve weeks post injection, animals received suprachoroidal electrode array implants in each eye, and responses to electrical stimulation were obtained using multiunit recordings from the visual cortex. Histologic measurements of neural and glial changes in the retina at the implant site were correlated with cortical thresholds from individual stimulating electrodes.

Results. Adenosine triphosphate-injected eyes displayed changes consistent with mid-to-late stage retinal degeneration and remodeling. A significant increase in electrical charge was required to induce a cortical response from stimulation of the degenerated retina compared to that in the fellow control eye. Spatial and temporal characteristics of the electrically evoked cortical responses were no different between eyes. Individual electrode thresholds varied in both the control and the ATP-injected eyes and were correlated with ganglion cell density. In ATP-injected eyes, cortical threshold was also independently correlated with an increase in the extent of retinal gliosis.

Conclusions. These data suggest that even when ganglion cell density remains unaffected, glial changes in the retina following degeneration can influence the efficacy of suprachoroidal electrical stimulation. A better understanding of how glial change impacts retinal prosthesis function may help to further the optimization of retinal implants.

Keywords: gliosis, retina, retinal degeneration, retinal prosthesis, retinitis pigmentosa

Retinitis pigmentosa refers to a family of degenerations characterized by gradual photoreceptor loss and eventually blindness. Although there are no currently available treatments that slow or prevent photoreceptor death, there have been considerable efforts over recent years to develop effective photoreceptor replacement therapies. Restoration of visual perception using electrical stimulation delivered through retinal implants has been recently reported by several groups and has now become a commercial reality.[1–6] For a retinal implant to be efficacious, it is critical that the output neurons of the retina, the retinal ganglion cells (RGCs), remain viable and capable of transmitting information to the brain.

Following photoreceptor loss, the remaining inner retina is known to undergo a series of changes that are collectively known as retinal remodeling.[7,8] In particular, following the loss of cones, corruption of inner retinal circuits occurs. Although electrical stimulation in blind humans has been shown to elicit the perception of phosphenes through a variety of electrode array placements,[3,9,10] the influence of inner retinal remodeling on achieving optimal visual restoration remains unclear. This is especially important for devices implanted into the subretinal or suprachoroidal space (i.e., farther away from the ganglion cells) because vision restoration using these electrode locations may be influenced more by the local integrity of circuits within the inner retina that need to be traversed before reaching the ganglion cells.[11] For example, there is recent evidence to suggest that a subretinal photovoltaic array generates electrophysiological responses in vivo in part through local activation of surviving bipolar cell circuitry in the degenerated rat retina.[12] Suprachoroidal placement of a retinal implant allows for a safe and straightforward surgical procedure as well as long-term mechanical stability; however, the location of the electrode array is even more distal to the retinal ganglion cells than that of subretinal implants and may therefore be more influenced by retinal remodeling.

Retinal implants placed in the suprachoroidal space between the sclera and choroid have been extensively studied in the normally sighted feline[13–18] and more recently in humans with retinitis pigmentosa[3,19] by our group. The effect of late-stage retinal remodeling events on device function is difficult to determine in human trials, because there is no way to compare blind retina implanted with a visual prosthesis with healthy human retina. There is some evidence that the extent of retinal degeneration influences cortical thresholds to retinal stimulation in a subretinal or trans-scleral retinal implant,[20,21] but no studies have examined what factors involved in retinal degeneration influence device efficacy. Thus, it is largely unclear if functional outcomes are due to the specific design, placement, or stimulation strategy of a device, or to the stage of disease progression in a patient, or to the result of some other factor. There remains the need to evaluate the efficacy of a clinical grade suprachoroidal implant in a large-eyed model of retinal degeneration, where the location of electrodes relative to the retina (and the effect of retinal remodeling on this positioning) is similar to that in human implants.

We have recently developed a feline model of unilateral retinal degeneration by intravitreal injection of adenosine triphosphate (ATP).[22,23] This model provides a unique opportunity to directly compare the effects of suprachoroidal stimulation in a degenerated retina with that in a normally sighted fellow eye within the same animal. The central aim of this study was to examine how loss of photoreceptors and associated retinal remodeling influences the efficacy of suprachoroidal retinal stimulation.

Materials and Methods

Anesthesia and Intraocular Injection of ATP

Adult felines ($n = 4$) were used in this study, and all had normal retinal function at baseline as demonstrated by electroretinogram (ERG). All four animals were a subset of a larger cohort ($n = 19$) required for another study[22] but were used for an acute electrophysiology experiment at the completion of the blinding period. Treatment of animals complied with the Association for Research in Vision and Ophthalmology Statement for Use of Animals in Ophthalmic and Vision Research and the National Health and Medical Research Council's "Australian Code of Practice for the Care and Use of Animals for Scientific Purposes" (2013) and the "Prevention of Cruelty to Animals Act" (1986; and amendments). The study was approved by the Royal Victorian Eye and Ear Hospital Animal Ethics Committee (Project 12/256AB).

Unilateral retinal degeneration was induced in all four animals by using a single intravitreal injection of ATP at a concentration of 11 mM at the retina as previously described.[22,24,25] We have previously found that ATP injection induces a global retinal degeneration with a variable pattern of photoreceptor loss, where the most severely affected inner retina occurs in regions containing fewer residual photoreceptor nuclei.[22,23] Briefly, the procedure was performed under anesthesia induced through a subcutaneous injection of ketamine (20 mg/kg; Ilium Ketamil; Troy Laboratories Pty. Ltd., Glendenning, NSW, Australia) and xylazine (2 mg/kg; Ilium Xylazil-20; Troy Laboratories). One eye was injected with a 200-μL solution of sterile phosphate-buffered saline (PBS; 0.9%) containing 0.2 M ATP hydrate to induce photoreceptor degeneration (Sigma Pharmaceuticals Ltd., Melbourne, VIC, Australia) and 0.2 mg dexamethasone to reduce inflammation (4 mg/mL dexamethasone; Aspen Australia, Sydney, NSW, Australia). As sham injections carried a slight risk of cataract formation and a comparison of sham injected and uninjected controls had previously found no differences,[22] the fellow eye was the uninjected control.

In Vivo Assessment of Retinal Thickness and Function

Retinal structure and function in the ATP-injected animals was assessed preinjection and at 12 weeks post injection. Animals were anesthetized using a subcutaneous dose of ketamine (20 mg/kg) combined with xylazine (2 mg/kg). Structure was assessed using optical coherence tomography (OCT) scans across the area centralis (Spectralis; HRA+OCT, Heidelberg Engineering, Heidelberg, Germany). Function was assessed using full-field, twin-flash ERG (Espion; Diagnosys LLC, Lowell, MA, USA) to separate the rod- and cone-pathway-mediated functions. All assessment and analysis methodologies performed in these animals have been described previously[22] and are similar to techniques used in other retinal prosthesis studies.[26–29]

Stimulating Electrode Array

The experiments described in this study used a stimulating electrode array with a similar design to the arrays used in our phase I clinical trial[3] that was surgically placed in the suprachoroidal space (Fig. 1), as described previously.[17,30] The array was designed to conform to the curvature within the suprachoroidal space and consisted of 21 platinum stimulating electrodes 600 μm in diameter, on a 17-mm by 8-mm silicone substrate (Fig. 1A). The electrodes were arranged hexagonally in 3 offset columns and spaced at a distance of 1 mm from center to center. Two larger platinum return electrodes, each 2 mm in diameter, were located distal to the stimulating electrodes. Figures 1B and 1C show representative fundus images in the ATP-injected (Fig. 1B) and fellow control (Fig. 1C) eyes of one animal with the approximate position of each stimulating electrode on the suprachoroidal electrode array overlaid over the fundus outline. The location of the area centralis in the fundus was determined by cross-referencing the location with infrared reflectance fundus and OCT images taken during clinical assessment (see Aplin et al.[22] for an example of infrared reflectance fundus).

Surgical Implantation of Stimulating Electrode Array

Following clinical assessments at 12 weeks post ATP injection, animals received suprachoroidal stimulating electrode array implants in both eyes. Animals were initially anesthetized by using a subcutaneous dose of combined ketamine (20 mg/kg) and xylazine (2 mg/kg) and maintained under anesthesia using an intravenous infusion of sodium pentobarbitone (aka pentobarbital) (60 mg/kg/h; Troy Laboratories). Both the sighted and the ATP-injected eye received electrode array implants of identical design, using a previously described surgical procedure.[14–18,29] Briefly, the suprachoroidal space was exposed through a lateral canthotomy, followed by a scleral incision. In order to allow for device implantation, a tissue pocket was created in the suprachoroidal space. The suprachoroidal array was then inserted 15 to 17 mm into the tissue pocket and externally sutured to the sclera (8/0 nylon sutures; Johnson & Johnson, Sydney, NSW, Australia). Each array was implanted as close to the area centralis as possible in order to facilitate comparable thresholds between the degenerated and control eyes. The relative retinal position of the implanted arrays was assessed using a fundus lens (Quadraspheric fundus lens; VolkH, Mentor, Ohio, USA) and surgical microscope (OPMI 6-CFR XY; Carl Zeiss AG, Gottingen,

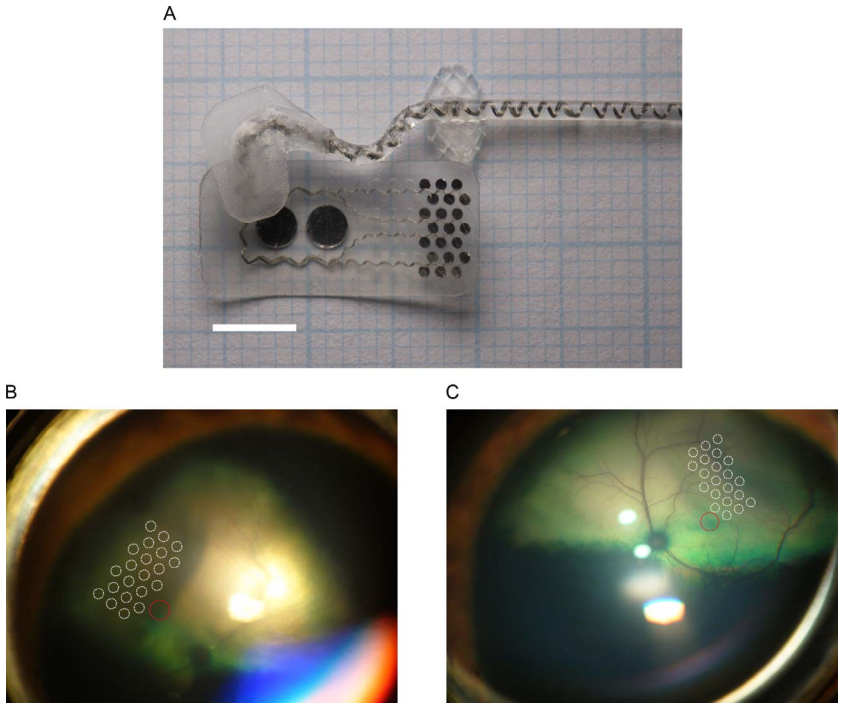

FIGURE 1. Suprachoroidal stimulating array. (**A**) Suprachoroidal prosthesis used for retinal stimulation in this study. The two return electrodes are on the *left* of the image, and the 21 stimulating electrodes are on the *right*, with the lead wire leaving the image on the *right side*. *Scale bar*: 5 mm. (**B**, **C**) Representative fundus photographs in one animal, showing the approximate location of each stimulating electrode on the suprachoroidal array implanted in an ATP-injected (**B**) and fellow control (**C**) eye (**C**). *Red circles* indicate approximate location of the area centralis in each eye.

Germany) fitted with a beam splitter and camera mount (Carl Zeiss). No modifications to the surgical procedure were necessary to accommodate retinal degeneration present in the ATP-injected eye.

Cortical Electrophysiology

Immediately after implantation of the suprachoroidal electrode arrays at 12 weeks post injection, the animal was fitted to a stereotaxic frame (David Kopf Instruments, Tujunga, CA, USA), and a craniotomy was performed to expose both visual cortices. Electrode impedances were measured in each eye after implantation at the end of the cathodic phase of a biphasic current pulse and defined as the peak electrode voltage divided by the current.[16] The most sensitive region in each cortical hemisphere in response to electrical stimulation of the retina was determined by recording local field potentials over the cortical surface.[13] Custom-designed arrays used for recording these potentials consisted of an 8×4 grid of platinum electrodes on a highly flexible thin-film polyimide substrate.[31] Following this, a 6×10 multielectrode penetrating array (Blackrock Microsystems, Salt Lake City, Utah, USA) was implanted in each visual cortex. The microelectrode penetrating arrays sampled a cortical area of 2 mm mediolaterally by 3.6 mm caudorostrally to a depth of ~1 mm and recorded multiunit spiking activity. Electrical stimulation and recording protocols were similar to those used by our group previously.[15–18] Electrodes on the retinal array were stimulated in a randomized order with cathodic-first, charge-balanced single biphasic pulses at defined current levels up to a maximum charge density of 300 $\mu C/cm^2$ (10 repetitions at each current level) and 3 phase durations (250, 500, and 1000 μs). An interphase gap of 25 μs was used in all conditions, and pulses were presented at a rate of 1 Hz. Band pass-filtered (300–5000 Hz) multiunit activity was recorded from each cortical hemisphere, thus analysis of response properties for each eye included both the contralateral and the ipsilateral cortex. Data were cleaned (electrical artifacts removed) offline and analyzed using customized scripts in Igor Pro (Wavemetrics, Tigard, OR, USA) (Fig. 2A).[32] A significant, stimulation-induced multiunit spike event was considered to have occurred whenever the signal exceeded 4.2 times the root-mean-square of the background noise.[13,16] Spikes were then plotted as a peristimulus time histogram in 0.1-ms bins in a 400-ms window (Fig. 2B) and a 20-ms window (Fig. 2C). Spikes counted in a window 3 to 20 ms post stimulus were plotted relative to each current level at each cortical location and fitted to a sigmoid curve (Fig. 2C). A 3- to 20-ms window was chosen in order to capture most of the retinal ganglion cell (short latency) and inner retinal-mediated (medium latency) activities as reported by Boinagrov et al.,[33] while reducing the possibility that cortical feedback might confound spike analysis, and maintaining a consistent analysis window with previous studies. A preliminary analysis of longer windows, up to 400 ms, did not reveal activity beyond 20 ms that had the capacity to significantly contribute to cortical threshold. A number of cortical measurements were then quantified.

First, threshold was defined as the current level required to elicit 50% of the maximum firing rate for a particular cortical electrode (Fig. 2C). The 50% activation point was chosen as it is the steepest point on the sigmoid curve and therefore has the least error in estimation.[32] The lowest recorded cortical threshold for each stimulating electrode was designated as the threshold for that stimulating electrode, and the corresponding cortical recording electrode was designated as its best cortical electrode (BCE).[17,18]

Second, latency for a given cortical electrode was defined as the average time to first spike across 10 repetitions at the maximum current on a stimulating electrode. Third, the total yield for each stimulating electrode, calculated separately for each cortical hemisphere, was defined as the percentage of all

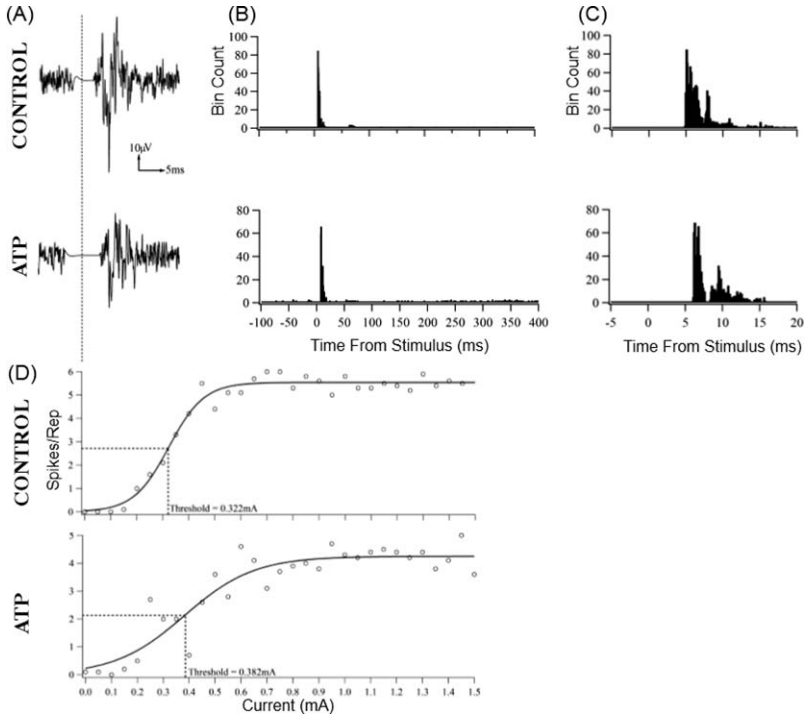

FIGURE 2. Electrophysiology acquisition and analysis. (**A**) Representative multiunit activity on single cortical channels from stimulating an electrode in control and ATP-injected eyes in one animal. (**B**, **C**) Representative 0.1-ms bin width PST histograms across all currents collating triggered spikes in response to a stimulus for each example in (**A**), using a 400-ms (**A**) and 20-ms (**B**) window. (**C**) Representative input-output functions of current versus spike rate within the 20- ms window, fitted to a sigmoidal curve for each example in **A**. *Dashed lines* indicate threshold, defined as the current required to elicit 50% of the maximum spike rate.

active implanted cortical electrodes that had a quantifiable threshold to stimulation.

We did not perform any spike-sorting procedures and analyzed the data as multiunit activity representing a population response at each recording site. This approach was chosen so our results could be directly compared to those of all our previous studies involving suprachoroidal stimulation in normally sighted cats,[16,34] as well as to keep consistent with other studies performing epiretinal and subretinal stimulation in normally sighted cats,[35,36] where it has been shown that cortical multiunit activity is an effective measurement with which to estimate thresholds and spatial resolution obtainable with a retinal implant.

A cortical spatial map was also generated for each stimulating electrode by plotting the spike rate across all recording electrodes at the current level required to reach 90% of the maximum spike rate on the BCE. Spike rates for each cortical electrode were normalized to their own maximum recorded spike rate to any stimulus. In order to measure the spread of cortical activation, cortical selectivity was calculated for each spatial map.[17,18] Cortical selectivity for each stimulating electrode was measured as the rate of reduction in normalized spike rate across the cortex as a function of physical distance from the BCE, quantified by taking the inverse tau of a decaying exponential function fitted to a graph of spike rate versus distance from BCE.[17,18]

Tissue Collection and Histology

Animals were euthanized at the completion of the acute electrophysiology experiment (typically, 48–72 hours post implantation) by using an overdose of intravenous sodium pentobarbitone (60 mg/kg; Troy Laboratories). The suprachoroidal electrode arrays were removed from the suprachoroidal space as carefully as possible to avoid physical damage to the retina. Both of the eyes were then enucleated, and tissue anterior to the ciliary body was removed. The posterior eyecups were fixed in 4% paraformaldehyde for 30 minutes and washed in PBS. In order to match the histology to the implanted electrode position, the retina was dissected into perpendicular sections, advancing along the length of the suprachoroidal tissue pocket left by the implanted electrode (clearly visible as a darker area in the sclera beneath the retina), with the center of each section located at the center of the array pocket. Additionally, the size and location of the visible pocket were matched to fundus photographs taken post implantation to ensure accurate positioning. Sections were then equilibrated in graded solutions of sucrose (10%, 20%, and 30% w/v in PBS) for at least 30 minutes each and stored overnight. Control and ATP-treated tissue were embedded in optimal cutting temperature compound (Tissue-Tek, Torrance, CA, USA), frozen, and cut into 12-μm serial sections using a cryostat (Microm, Walldorf, Germany). Sections were collected on poly-L-lysine-coated slides (Menzel-Glaser, Braunschweig, Germany) and stored at −20°C. Sections were cut serially, with all missed sections accounted for, which allowed for a good approximation of electrode position by counting the number of micrometers advanced for each section. As each electrode "column" was spaced 1000 μm from center to center and sections were cut at 12-μm intervals, every 84 sections corresponded approximately to the offset center of an electrode column.

Indirect fluorescence immunohistochemistry was used to assess the extent of inner and outer retinal changes in the ATP-injected eyes and to quantify variations in retinal thickness and glial changes. Immunohistochemical techniques followed methodology previously described.[22,24] After fixation and sectioning, slides were defrosted and washed in PBS. Sections were incubated overnight at room temperature in antibody buffer (3% normal goat serum, 1% bovine serum albumin, 0.5%

Triton-X in PBS) containing 2 or 3 primary antibodies (listed below). The primary antibody solution was removed through repeated PBS washes, and the sections were incubated for 3 hours in antibody buffer containing secondary antibody diluted 1:500 (goat anti-mouse Alexa Fluor 488, goat anti-rabbit Alexa Fluor 594, or goat anti-guinea pig Alexa Fluor 643; Life Sciences, Melbourne, VIC, Australia) and a nuclear stain diluted 1:300 (4′,6-diamidino-2-phenylindole [DAPI; Life Sciences]). Sections were then washed in PBS and coverslipped with a polyvinyl alcohol (Mowiol)-based antifade mounting medium (Polysciences, Inc., Warrington, PA, USA) and photomicrographs taken using a laser scanning confocal microscope (Leica Microsystems, Sydney, NSW, Australia) with a 20× air or 40× oil objective. The appropriate fluorescence filters were used (Alexa 594/Cy3 excitation, 568 nm; emission, 605/32; Alexa 488/fluorescence-activated cell sorting excitation, 488 nm, emission, 522/32) for visualization of the fluorophores.

In order to examine survival and reorganization of the outer retina, retinae were labeled with mouse anti-Rho 4D2 (R4D2; 1:50 dilution; Abcam, Cambridge, UK), combined red/green and blue rabbit anti-cone opsin (1:500 dilution; Millipore, Melbourne, VIC, Australia) and Fluorescent labeled peanut agglutinin (PNA; 1:200 dilution; Vector Laboratories, Crofton, MD, USA). Rho4D2 labels rhodopsin in rod photoreceptors in the feline.[37] Cone opsin labels the opsins in cone photoreceptors in the feline.[38] PNA labels the structure galactosyl(b1,3) *N*-acetylgalactosamine found in cone photoreceptor inner and outer segments in the feline.[38] In order to examine the effect of ATP-induced degeneration on the neurons of the inner retina, retinae were labeled with mouse anti-calretinin (1:500 dilution; Swant, Bellinzona, Switzerland) and guinea pig antivesicular glutamate transporter (VGLUT1; 1:1000 dilution; Millipore). calretinin labels a small subset of ganglion cells, horizontal cells, and a subset of amacrine cells in the feline, most notably the AII amacrine cell population.[39,40] VGLUT1 labels photoreceptor and bipolar cell terminals.[41] In order to examine the effect of ATP-induced retinal degeneration on Müller cell and astrocyte morphology, retinae were labeled with rabbit anti-glial fibrillary acid protein (GFAP; 1:10,000 dilution; Dako, Carpinteria, CA, USA). GFAP reliably labels astrocytes and gliotic Müller cells in the retina, as well as a small percentage of normal functioning Müller cells in the feline.[42–44] In order to examine retinal ganglion cell survival, retinae were labeled with anti-RNA-binding protein with multiple splicing (RBPMS). RBPMS consistently labels retinal ganglion cell somas across multiple species and has previously been tested in mouse, rat, guinea pig, rabbit, and monkey retina.[45]

We quantified local variations in retinal thickness and retinal ganglion cell density across the implanted section of retina by using sections labeled for GFAP or RBPMS and DAPI as detailed above. Sections were imaged with a laser scanning confocal microscope (Leica) with a 20× air objective. Individual scans were combined into a tiled image and measured using ImageJ software (version 1.48, http://imagej.nih.gov/ij/; provided in the public domain by the National Institutes of Health, Bethesda, MD, USA), using a customized script. Layer thicknesses were measured in sets of 5 repeats spaced at 100-μm intervals, with each set separated by 1000 μm starting from the center of the section. Thicknesses were defined as "total retinal thickness" (measured from the retinal nerve fiber layer to the last row of inner or outer layer nuclei), "outer nuclear layer thickness" (from the first to the last row of outer nuclear layer nuclei, or recorded as none if no nuclei were present), and "GFAP thickness" (total pixel area of the total retinal thickness measurement that had positive GFAP). Retinal ganglion cell density was measured by manually counting RBMPS-labeled cell bodies in 1000 μm bins starting from the center of the section.

Statistical Analysis

Analyses were performed using cortical thresholds, spatial selectivity, and histologic comparisons in eyes injected with ATP compared to control eyes (using Prism v.4 software [Graphpad, LaJolla, CA, USA]; SigmaPlot v12.5 [Systat Software, San Jose, CA, USA]; and Stata Statistical Software v. 13 [StataCorp., College Station, TX, USA]) within each animal. Results are expressed as mean ± standard error of the mean (SEM) unless otherwise noted. All data were analyzed using a Shapiro-Wilk test for normality. As our data were nested (thresholds obtained within eye, within animal), it was not always possible to perform ANOVA to determine statistical significance.[46] Thus, in order to account for the correlation between eyes and between electrodes in an eye, as well as colinearity and potentially missing data, we used a mixed-effects general linear model (GLMM).[47] For a comparison of thresholds, selectivity, and first-spike latencies between treatments, the phase width and eye status were considered fixed effects, while the electrodes nested in each eye, nested in each animal, were considered a random effect. Histologic correlations were analyzed separately for each treatment with total retinal thickness, outer nuclear layer thickness, GFAP expression thickness, and retinal ganglion cell count as fixed effects and animal as a random effect. Data without a nested component were analyzed by a 2-way ANOVA (for cortical yields) or unpaired Student's *t*-test (for impedances and distance of implantation from area centralis). A Holm-Sidak post hoc test was used to determine significance for multiple pairwise comparisons. Details of individual tests used are also provided in the results. In all figures, statistical significance is expressed as $P < 0.05$.

Results

Intravitreal ATP Injection Induces Retinal Degeneration in the Feline

We confirmed that, prior to the acute electrophysiology experiments, all animals had undergone similar levels of unilateral photoreceptor degeneration as a result of intravitreal injection of ATP. Figures 3A and 3B show representative rod- and cone-mediated ERG waveforms extracted from a twin-flash paradigm prior to ATP injection and at 12 weeks post injection. There were substantial decreases in rod-mediated and cone-mediated retinal functions 12 weeks following injection with ATP. There was a decrease of approximately 80% in rod-mediated a-wave amplitude and an 85% decrease in cone-photoreceptor mediated a-wave amplitude compared with preinjection twin-flash ERG responses (Fig. 3E), with a range of ~70% to 90% loss in rod a-wave amplitude and 80% to 100% loss in cone a-wave amplitude across the 4 experimental animals. Using OCT, we confirmed that there was a loss of photoreceptor nuclei in the outer nuclear layer (ONL) following ATP injection by examining retinal structure within the area centralis (Figs. 3C, 3D). One eye was unable to be analyzed using OCT because of an intense inflammatory response that obscured the retina. Outer nuclear layer thickness was significantly reduced in all eyes treated with ATP, and total retinal thickness remained well conserved (Fig. 3E). A preservation of total retinal thickness greater than overall loss of ONL could potentially be due to retinal swelling or gliotic proliferation.[22] In order to assess how much our measure of total thickness might be influenced by gliosis in the retina, we measured the total percentage of retina taken up by either ONL nuclei or tissue positive for GFAP localization in both control and ATP- treated retinae (Fig. 3F). GFAP-positive

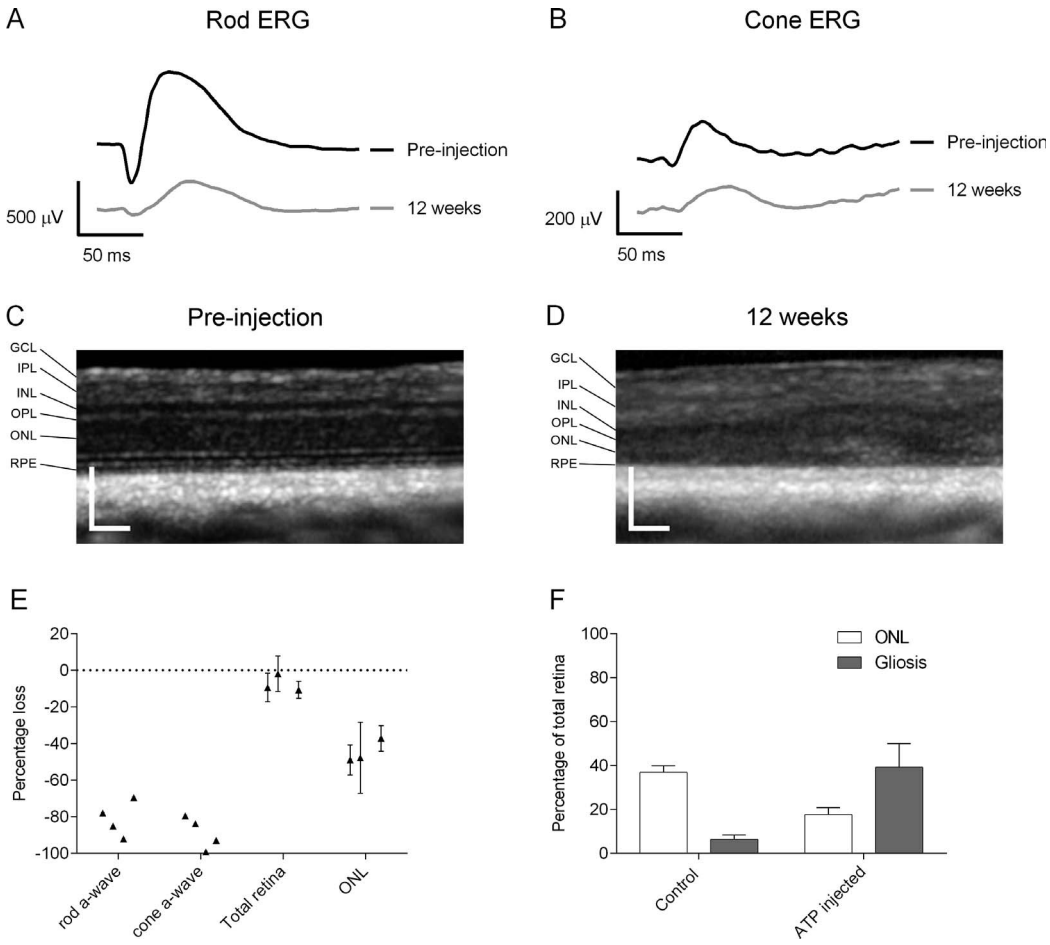

Figure 3. Adenosine triphosphate-induced retinal degeneration in the feline. (**A**, **B**) Representative ERG waveforms show isolated rod (**A**) and cone (**B**) responses preinjection and at 12 weeks post injection. Note different voltage scales used for rod and cone responses. (**C**, **D**) Representative OCT images across the area centralis preinjection (**C**) and at 12 weeks post injection (**D**). (**E**) Percentage of loss of isolated rod and cone a-wave amplitudes, OCT total retinal thickness, and OCT outer nuclear layer thickness in ATP-injected eyes at 12 weeks. Individual data points represent values from each experimental animal. One animal was excluded from the OCT analysis due to intraocular inflammation that prevented an accurate OCT scan. *Error bars*: 1 SD from the mean. (**F**) Percentage of contribution of total retinal thickness by ONL nuclei and GFAP-positive tissue. *Scale bar*: 200 μm. GCL, ganglion cell layer; IPL, inner plexiform layer; INL, inner nuclear layer; OPL, outer plexiform layer; ONL, outer nuclear layer; RPE, retinal pigment epithelium.

cells comprised nearly half of the neural retina in ATP-treated tissue, more than compensating for the reduction in ONL thickness. Thus, the preservation of total retinal thickness was likely the result of greatly increased gliotic activity in the retina and may not reflect maintained retinal function. This is consistent with previous reports showing that increased inner retinal thickness contributed to total retinal thickness despite loss of photoreceptors in ATP-injected eyes.[22] In one animal, there was a localized retinal detachment in the distal nasal retina far from the region of the implanted array; otherwise this general pattern of photoreceptor nuclear layer thinning was consistent across the entire retina. For a more comprehensive analysis of the ERG waveform and retinal thicknesses in the ATP-injected feline, of which these animals are a subset, refer to Aplin et al.[22] These data confirmed that a single injection of ATP induced photoreceptor loss and loss of retinal function within 12 weeks in all implanted animals.

Retinal Degeneration Leads to Increased Cortical Thresholds in Response to Retinal Simulation

Having established that ATP had induced unilateral degeneration, animals underwent implantation of suprachoroidal stimulating electrode arrays in both eyes, and cortical activity in response to retinal stimulation was recorded over a 3- to 4-day period. We first confirmed that impedances of the stimulating electrodes were not significantly different in the two experimental groups (mean control impedance = 11.711 ± 1.117 kΩ; mean ATP-injected impedance = 11.244 ± 2.02 kΩ; unpaired Student's *t*-test; $P = 0.844$; $n = 76$ retinal electrodes in the control eyes and 84 retinal electrodes in the ATP-treated eyes).

Electrically evoked multiunit activity from the visual cortex was analyzed from 450 of 960 cortical recording sites implanted across all experiments. In all animals, there was a high percentage (>80%) of functioning stimulating suprachoroidal electrodes evoking enough cortical activity to measure threshold on at least one recording electrode (Fig. 4A). There were no significant differences in the percentages of stimulating electrodes with enough activity to measure threshold in each animal between ATP-injected and control eyes (2-way ANOVA, $F = (2, 18)$; $P = 0.421$; $n = 4$ animals), and this was consistent when using all phase widths for stimulation (2-way ANOVA; $F = (2, 18)$; $P = 0.488$; $n = 4$ animals).

Figure 4B shows the mean best cortical electrode threshold (calculated in charge per phase) for stimulation in ATP-injected and control eyes. Longer phase durations elicited higher cortical thresholds in both ATP-injected and control eyes

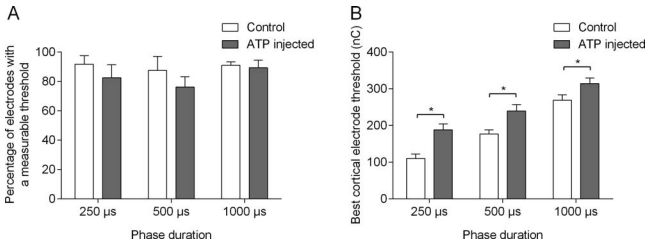

Figure 4. Cortical thresholds increased in ATP-induced retinal degeneration. (**A**) Percentage of retinal electrodes with a cortical threshold in control and ATP-injected eyes, using 250-, 500-, and 1000-µs phase durations. (**B**) Mean cortical threshold (charge per phase in nC) in response to suprachoroidal stimulation in control and ATP-injected eyes, using 250-, 500-, and 1000-µs phase durations. Threshold varied with eye status (GLMM $P < 0.001$; $n = 42$–75 retinal electrodes) and phase duration (GLMM $P < 0.001$; $n = 42$–75 retinal electrodes, * in [**B**]). nC = nanocoulombs.

compared to shorter phase durations (GLMM $P < 0.001$; $n = 42$ control 250 µs; 49 ATP 250 µs; 64 control 500 µs; 64 ATP 500 µs; 72 control 1000 µs; 75 ATP 1000 µs retinal electrodes). Regardless of phase duration, ATP-injected eyes showed significantly higher cortical thresholds in response to retinal stimulation compared to controls (GLMM $P < 0.001$; $n = 42$ control; 250 µs; 49 ATP 250 µs; 64 control 500 µs; 64 ATP 500 µs; 72 control 1000 µs; 75 ATP 1000 µs retinal electrodes).

Retinal Degeneration Influences Location of Cortical Responses to Stimuli but not Spatial Selectivity

Figure 5A shows representative cortical spatial maps (contralateral hemisphere for control eye, ipsilateral hemisphere for ATP eye) induced by stimulating a single retinal electrode in an ATP-injected and control eye in one animal. From this the rate of reduction in spike rate across the cortex as a function of physical distance from the best cortical electrode (cortical selectivity) was inferred (Fig. 5B). Cortical selectivity (Fig. 5C) did not vary between ATP-injected and control eyes (GLMM $P = 0.694$; $n = 42$–75 retinal electrodes) or with phase duration (GLMM $P = 0.894$; $n = 42$–75 retinal electrodes). We also quantified the time it took for retinal stimulation to induce cortical activation (first spike latency). There was no variation in cortical first spike latency between ATP-injected and control eyes, or with phase duration (average latency = 4.40 ± 0.12 ms in ATP-injected eyes and 4.52 ± 0.10 ms in control eyes; GLMM for ATP versus control eyes, $P = 0.957$; for phase duration, $P = 0.497$; $n = 42$–75 retinal electrodes).

We then examined the location of the BCEs for each stimulating retinal electrode. Given that temporal fibers cross to the contralateral hemisphere near the area centralis in the cat,[48,49] we predicted that the contralateral cortex would be the primary site of cortical activation. Figure 6A shows the percentage of BCEs in the contralateral cortex compared to those in the ipsilateral cortex for ATP-injected eyes and control eyes, using a 500-µs phase duration stimulus across 60 cortical electrodes per animal per hemisphere. As expected, there were more BCEs located in the contralateral cortex (~90%) than in the ipsilateral cortex (~10%) when stimulating the control eyes (2-way ANOVA; Holm-Sidak post hoc analysis; $F = (1, 12)$; $P = 0.003$; $n = 4$ animals). However, in ATP-injected eyes, there were no significant differences in contribution to BCE thresholds between the contralateral and ipsilateral cortexes (2-way ANOVA; Holm-Sidak post hoc analysis; $F = (1, 12)$; $P = 0.065$; $n = 4$ animals). In addition, BCE contribution between the two hemispheres did not vary with phase

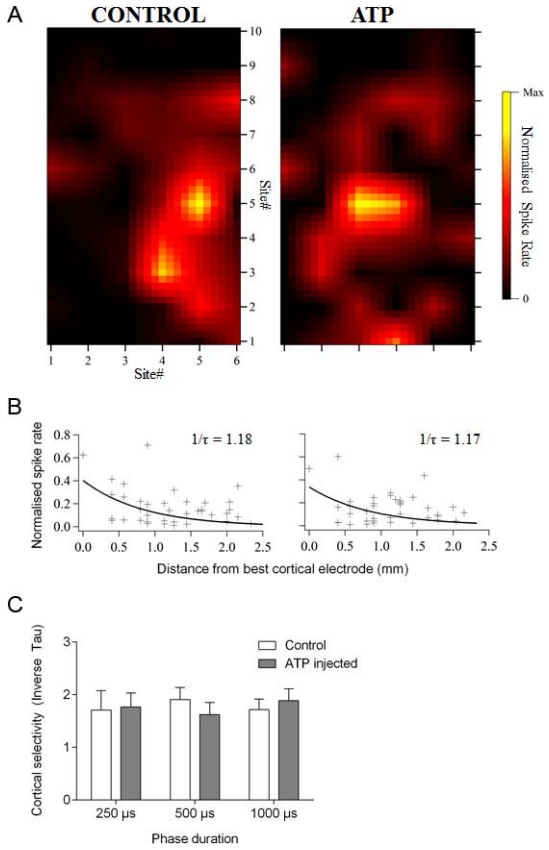

Figure 5. Retinal degeneration did not influence cortical selectivity (spread of activation). (**A**) Representative cortical spatial maps from the same cortical hemisphere from stimulating a single retinal electrode in an ATP-injected and fellow control eye in one animal, using a 500-µs phase duration. (**B**) Function of spike rate versus distance from the best cortical electrode was taken from the representative cortical spatial maps. Cortical selectivity was defined as the inverse tau of a decaying exponential fitted to this function. (**C**) Average cortical selectivity in control and ATP-injected control eyes, using 250-, 500-, and 1000-µs phase durations. Cortical selectivity did not vary between ATP-injected and control eyes (GLMM $P = 0.694$; $n = 42$–75 retinal electrodes) or with phase duration (GLMM $P = 0.894$; $n = 42$–75 retinal electrodes).

duration of the stimulus (data not shown; 2-way ANOVA; $F = (2, 18)$; $P = 0.779$; $n = 4$ animals).

In order to further explore this result, we assessed cortical activation in the form of the cortical yield, defined as the percentage of active cortical electrodes with a threshold in response to stimulation. Figure 6B shows cortical yield in the contralateral and ipsilateral cortices from stimulating ATP-injected eyes and control eyes with a 500-µs phase duration. In control eyes, there was significantly more activation in the contralateral cortex than in the ipsilateral cortex, as predicted (GLMM Holm-Sidak post hoc analysis, $P < 0.001$; $n = 64$ retinal electrodes). The ratio of contralateral-to-ipsilateral activation in fellow eye controls was also similar to that in bilaterally sighted animals analyzed in previous studies (data not shown; $n = 21$ retinal electrodes).[16] However, in ATP-injected eyes, there was significantly more activation in the ipsilateral cortex than in the contralateral cortex (GLMM Holm-Sidak post hoc analysis, $P = 0.005$; $n = 64$ retinal electrodes), and this was not dependent on phase duration (data not shown; GLMM $P = 0.638$ in the contralateral cortex, $P = 0.229$ in the ipsilateral cortex; $n = 42$–75 retinal electrodes). The percentage of cortical recording electrodes with a measurable threshold to stimulation of any given retinal electrode ranged considerably from 0 to 100%

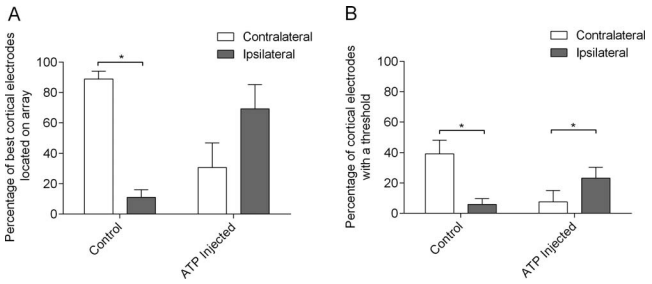

Figure 6. Retinal degeneration influenced location of activation in the cortex. (**A**) Relative contralateral and ipsilateral locations of best cortical electrode thresholds using a 500-μs phase duration, expressed as percentage of total of all cortical electrodes with a threshold. Significantly more BCEs were located in the contralateral cortex than in the ipsilateral cortex when stimulating control eyes. This was not observed when stimulating ATP-injected eyes (2-way ANOVA; Holm-Sidak post hoc analysis; $F = (1,12)$; $P = 0.003$; $n = 4$ animals). (**B**) Cortical yield in the contralateral and ipsilateral cortexes, expressed as the percentage of active cortical electrodes with a threshold in response to suprachoroidal stimulation. There were significant differences in cortical yield between the contralateral cortex and the ipsilateral cortex when stimulating control eyes (GLMM Holm-Sidak post hoc analysis; $P < 0.001$; $n = 64$ retinal electrodes) and ATP-injected eyes (GLMM Holm-Sidak post hoc analysis; $P = 0.005$; $n = 64$ retinal electrodes), but the ratio of contralateral-to-ipsilateral activation was markedly different for the two eye conditions. There were also significant differences in cortical yield between the control and ATP-injected eyes for both of the cortical hemispheres (GLMM Holm-Sidak post hoc analysis; $P = 0.008$; $n = 64$ retinal electrodes).

(contralateral hemisphere) and 0% to 58% (ipsilateral hemisphere) when stimulating control eyes and from 0 to 52% (contralateral hemisphere) and 0 to 78% (ipsilateral hemisphere) when stimulating the ATP-injected eyes.

Retinal Characteristics that Influenced Cortical Activation in Response to Stimulation

Thresholds of cortical responses were correlated to local variations in retinal structure to examine their relative contribution to the differences in cortical response. In order to account for the possibility that differences in surgical placement might account for the observed variation in thresholds, we first evaluated whether the average distance from the implanted array to the area centralis was different between control and ATP-injected eyes. In order to quantify the surgical location, we used fundus photographs that showed the position of the array after implantation (Figs. 1B, 1C), using the diameter of the optic disc as a consistent unit of distance between images. Electrodes in the ATP-injected eyes were not significantly closer to the area centralis than in control eyes (mean = 5.028 ± 0.1475 optic disc diameters in controls; mean = 4.377 ± 0.1377 optic disc diameters in ATP-injected animals; unpaired Student's *t*-test, $P = 0.3537$; $n = 4$ animals).

We evaluated the extent of neural and glial changes present as a result of ATP-induced photoreceptor degeneration (Figs. 7A–7G). One control eye was excluded from the analysis due to damage caused by an incision error during dissection. Figures 7A and 7B shows representative vertical sections of cat retinae labeled for cell nuclei (Fig. 7, DAPI blue), rhodopsin (Fig. 7, R4D2 pink), cone opsins (Fig. 7, cone opsin red), and cone outer segments (Fig. 7, PNA green) in a control (Fig. 7A) and an ATP-injected eye (Fig. 7B) after explantation of the suprachoroidal devices. In the control retina, rhodopsin and cone opsin labeling were confined to the outer segments of the photoreceptor layer, with no staining of cell bodies (Fig. 7A). In contrast, 12 weeks post ATP injection (Fig. 7B), the outer retina had become highly disorganized, with photoreceptor opsin primarily expressed in cell bodies, with few to no normal outer segments surviving. Furthermore, abnormal rhodopsin expression in photoreceptor cell bodies and evidence of photoreceptor cell migration were seen (Fig. 7B, horizontal arrowhead). Figures 7C and 7D show representative vertical sections of feline retinae labeled for cell nuclei (Fig. 7, DAPI blue), synaptic terminals (Fig. 7, VGLUT1 red) and amacrine, ganglion cell and horizontal cells (calretinin green) in a control (Fig. 7C) and an ATP-injected eye (Fig. 7D) under the implanted area. VGLUT and calretinin expression in the outer nuclear layer showed aberrant neurite outgrowth (Fig. 7D, vertical arrowheads), a loss of synaptic terminals in the inner and especially outer plexiform layers, and the migration of synaptic terminals into the ONL. Figures 7E and 7F show representative vertical sections of feline retinae labeled for cell nuclei (Fig. 7, DAPI; blue) and retinal ganglion cells (Fig. 7, RBPMS red) in a control (Fig. 7E) and an ATP-injected eye (Fig. 7F). Retinal ganglion cells appeared relatively well conserved compared to other retinal cell populations, with no qualitative changes in density or gross morphology. Figures 7G and 7H shows representative vertical sections of feline retina labeled for cell nuclei (Fig. 7, DAPI blue) and astrocytes and/or gliotic Müller cells (Fig. 7, GFAP; red) in an implanted control (Fig. 7G) and in an ATP-injected eye (Fig. 7H) directly beneath a single stimulating electrode. In many areas, Müller cells had undergone severe remodeling forming a glial scar structure both at the boundaries of the degenerate retina and occasionally infiltrating through the retina (Fig. 7H, vertical arrows). These features could be observed throughout the degenerated retinae and were not constrained to the implanted region. Thinning of the ONL was also apparent in the ATP-injected retina compared to the fellow control; however, there was variation in the severity of the degeneration across the retina.

Previous analysis using OCT in ATP-injected eyes revealed a variation in thickness of the outer nuclear layer and cells in the vitreous that suggested potential regional inflammation.[22] We thus predicted that cortical thresholds in the ATP eyes could vary significantly depending on the extent of photoreceptor loss, gliosis, or local density of the target neural population (retinal ganglion cells). Retinal thicknesses, gliosis and ganglion cell densities were determined at the approximate location of each electrode by analyzing 12-μm serial sections cut perpendicularly to the array pocket that were double-labeled with the nuclear stain DAPI and either the glial marker GFAP or the retinal ganglion cell marker RBPMS (Figs. 7E–7H). In order to allow for a visual comparison between the OCT and histologic data, as well as to account for the possibility of tissue shrinkage and oblique sectioning, the histologic thicknesses were normalized to OCT retinal thickness across the implanted area. This did not change the outcome of the statistical analyses. Figure 8 shows normalized total retinal thickness (Figs. 8A–8B), ONL thickness (Figs. 8C, 8D), GFAP expression thickness (Figs. 8E, 8F), and retinal ganglion cell density (Figs. 8G, 8H) plotted against electrode BCE threshold in 4 ATP-injected and 3 fellow eye controls, using a stimulus phase duration of 500 μs. Mean GFAP expression thickness was significantly increased, and ONL thickness was significantly reduced in ATP-injected animals compared to controls (GLMM $P < 0.001$; control $n = 48$ retinal electrodes; ATP $n = 64$ retinal electrodes). A general linear mixed-effects model was then used to assess correlations between histologic factors (control $n = 48$ retinal electrodes; model $r^2 = 0.49$; ATP $n = 64$ retinal electrodes; model $r^2 = 0.73$). Total retinal thickness and retinal ganglion cell count did not significantly vary between the two conditions (GLMM total retinal thickness $P = 0.813$; RGC count $P = 0.092$; $n = 48$ control; 64 ATP retinal electrodes). Total

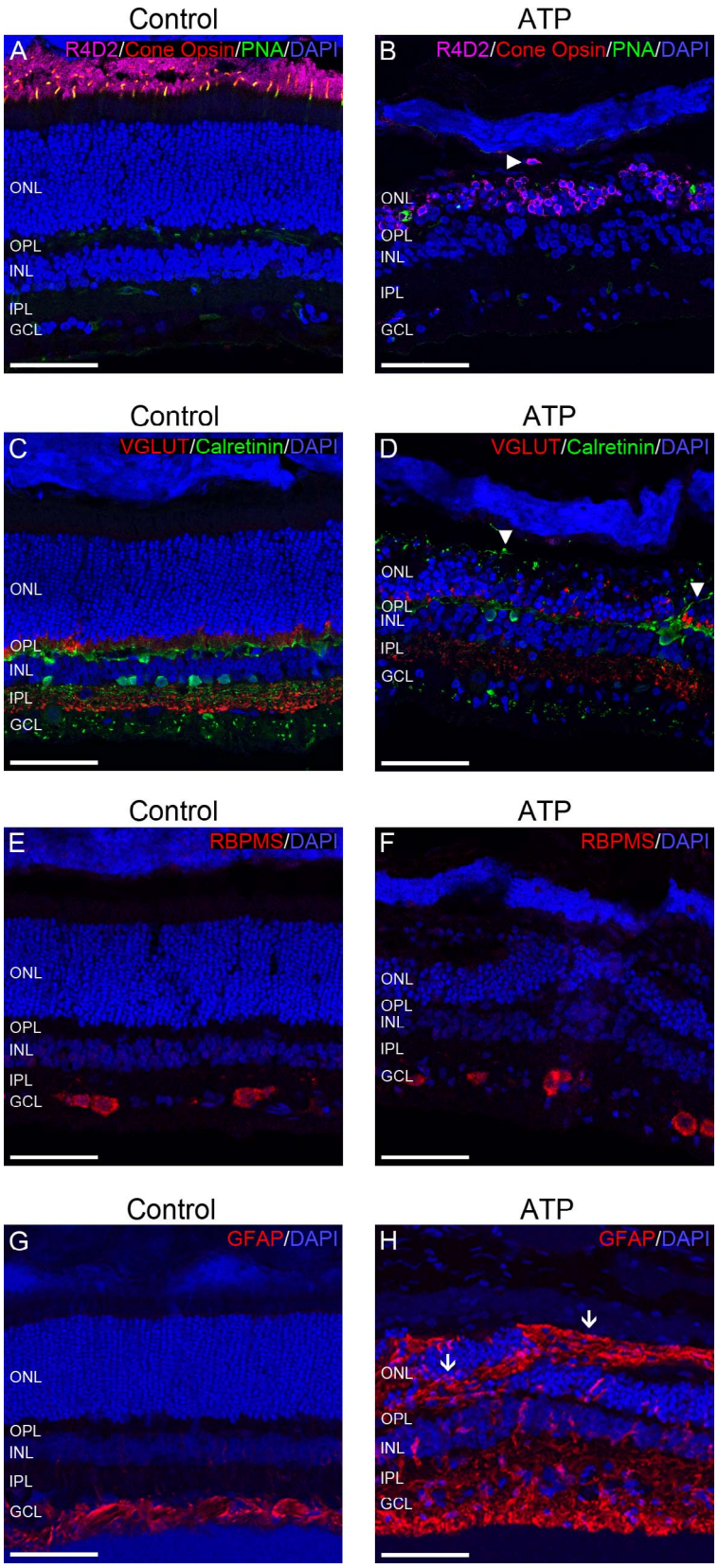

Figure 7. Retinal changes in response to ATP-induced photoreceptor degeneration. (**A**, **B**) Representative sections of control (**A**) and ATP-injected retinae (**B**) after device explantation, labelled for rhodopsin (R4D2 [*pink*]), cone opsins (*red*), cone outer segments (PNA [*green*]), and cell nuclei (DAPI [*blue*]). Horizontal *arrowhead* (**B**) indicates aberrant photoreceptor migration. (**C**, **D**) Representative sections of control (**C**) and ATP-injected retinae (**D**) labelled for glutamatergic synapses (VGLUT1 [*red*]), a subset of horizontal, amacrine, and ganglion cells (calretinin [*green*]), and cell nuclei (DAPI [*blue*]). Vertical arrowheads (**D**) indicate abnormal neurite growth into the outer retina. (**E**, **F**) Representative sections of control (**E**)

Investigative Ophthalmology & Visual Science

and ATP-injected (**F**) retinae labelled for retinal ganglion cells (RBPMS [*red*]) and cell nuclei (DAPI [*blue*]). (**G**, **H**) Representative sections of retinae directly underneath a stimulating electrode from a fellow control (**G**) and an ATP-injected (**H**) eye, labelled for cell nuclei (DAPI [*blue*]) and astrocytes or Müller cell gliosis (GFAP [*red*]). Vertical *arrows* (**G**) indicate regions of glial scar formation around and through the outer retina. GCL, ganglion cell layer; INL, inner nuclear layer; IPL, inner plexiform layer; ONL, outer nuclear layer; OPL, outer plexiform layer. *Scale bars*: 100 μM.

retinal thickness did not correlate with BCE threshold in either control or ATP-injected eyes (Fig. 8A–B; GLMM Control $n = 48$ electrodes; $r^2 = 0.10$; $P = 0.514$; ATP $n = 64$ electrodes; $r^2 = 0.24$; $P = 0.482$). Outer nuclear layer also did not correlate with BCE threshold in control or ATP-injected eyes (Figs. 8C, 8D, GLMM control $n = 48$ electrodes; $r^2 = 0.07$; $P = 0.735$; ATP $n = 64$ electrodes; $r^2 = 0.08$; $P = 0.166$). GFAP expression did not correlate with BCE threshold in control eyes but was strongly correlated with threshold in all ATP-injected eyes (Figs. 8E, 8F, GLMM control $n = 48$ electrodes; $r^2 < 0.01$; $P = 0.556$; ATP $n = 64$ electrodes; $r^2 = 0.28$; $P < 0.001$). Ganglion cell density also correlated with threshold in both control and ATP-injected eyes (Figs. 8G, 8H, GLMM control $n = 48$ electrodes; $r^2 = 0.02$; $P < 0.001$; ATP $n = 64$ electrodes, $r^2 = 0.02$, $P < 0.001$). In ATP-injected eyes there was significant colinearity between GFAP expression and RGC count (GLMM $P = 0.012$; $r^2 = -0.29$) and between total and ONL thicknesses (GLMM $P < 0.001$; $r^2 = 0.46$); these colinearities were accounted for as part of our statistical model, and all variance inflation factors < 5. As the amount of GFAP labeling increased or the density of retinal ganglion cells decreased, the amount of charge required to generate a threshold cortical response increased.

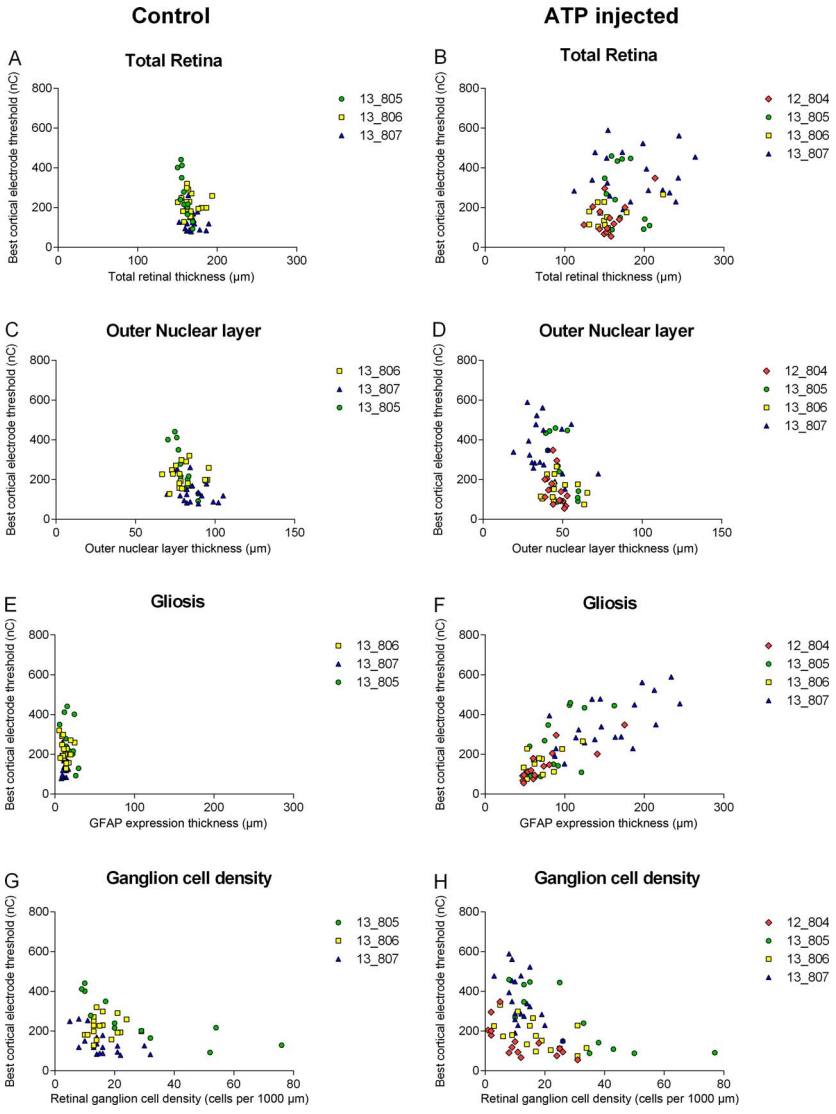

Figure 8. Electrode thresholds correlate with GFAP expression. (**A**, **B**) Total retinal thickness plotted against BCE threshold in control (**A**) and ATP-injected (**B**) eyes. (**C**, **D**) Outer nuclear layer thickness plotted against BCE threshold in control (**C**) and ATP-injected (**D**) eyes. (**E**, **F**) GFAP expression thickness plotted against BCE threshold in control (**E**) and ATP-injected (**F**) eyes. (**G**, **H**) Retinal ganglion cell density plotted against BCE threshold in control (**G**) and ATP-injected (**H**) eyes. All thresholds were obtained using a 500-μs phase duration. Each symbol and color combination corresponds to a single animal with a total of two suprachoroidal devices implanted (one in the ATP-injected eye and one in the fellow control eye). Ganglion cell density correlated with threshold in both the control and the ATP-injected eyes (GLMM control $n = 48$ electrodes; $r^2 = 0.02$; $P < 0.001$; ATP $n = 64$ electrodes; $r^2 = 0.02$; $P < 0.001$). GFAP expression correlated with threshold only in ATP-injected eyes (GLMM control $n = 48$ electrodes; $r^2 < 0.01$; $P = 0.556$; ATP $n = 64$ electrodes; $r^2 = 0.28$; $P < 0.001$).

Discussion

ATP-Induced Retinal Degeneration Influences the Efficacy of a Suprachoroidal Prosthesis

Using a feline model of unilateral retinal degeneration, we evaluated the effects of retinal stimulation on cortical responses from a degenerated and fellow control eye in the same animal. Intravitreal injection of ATP-induced photoreceptor loss within 12 weeks, which was consistent with previous work.[22] Suprachoroidal stimulation of degenerate and control retinae elicited responses in the cortex across all tested phase durations. In the degenerate retina, significantly higher levels of charge were required to generate a cortical response than to uninjected control retina. Cortical thresholds to suprachoroidal stimulation have been determined previously in the normally sighted feline,[13,16,18] and comparable thresholds were detected from stimulation of the control eyes in this study. Our previous studies acknowledged the possibility that photoreceptive responses to stimulation may have confounded analyses.[16,18] Based on recent data by Boinagrov et al.[33] and our present data including the short response latencies and lack of any correlation between residual outer nuclear layer thickness and cortical thresholds, we can confirm that photoreceptors are not the primary target cell population with suprachoroidal stimulation.

Although higher charges were required to elicit a cortical response to stimulation of the ATP-injected eye, it should be emphasized that the stimuli used were well within the safe charge limits. Less than half the theoretical maximal charge limit for stimulation per electrode with platinum electrodes was required to elicit a threshold cortical response to stimulation of the degenerate retina.[50–52] Other studies have reported a greater difference in stimulation threshold in degenerated eyes than in normal eyes.[20,21,53,54] This may represent differences in the animal model and level of degeneration and in vitro compared to in vivo stimulation paradigms used, as we would expect major differences in the type and location of the electrode array between the various studies. Nevertheless, our data show that retinal stimulation in an ATP-induced model of retinal degeneration is viable and can be elicited at charge thresholds that are higher but well within the safety limits of stimulating with platinum electrodes.

Chronic Retinal Degeneration May Influence the Pattern of Cortical Activation in Response to Retinal Stimulation

Although cortical thresholds differed between degenerate and control eyes, we did not observe any differences in cortical latency or cortical selectivity. Our results are consistent with those of another in vivo study in a rabbit model of retinal degeneration, in which there were no changes in the latency of cortical evoked potentials elicited by episcleral stimulation.[55] In addition, we observed cortical selectivity values similar to those reported in a previous study using normally sighted cats,[18] with no differences between control and ATP-injected eyes. These data suggest that, despite the higher charge required to induce cortical activity, the response latency and spatial spread of the neural signal at the cortex remains similar across cohorts.

We did observe a shift in the location of cortical responses, with a significant majority of responses from stimulating the ATP-injected eye coming from the ipsilateral cortex. This was unexpected as our retinal arrays were positioned in an area of the temporal retina where, in the feline, the majority of ganglion cells project to the contralateral brain[48,49,56] and our cortical recording array positions were each optimized for their corresponding contralateral eyes. One possible explanation is that the visual pathway downstream from the retina might have undergone reorganization in response to chronic unilateral retinal degeneration. Monocular deprivation in young mammals is capable of drastically influencing the strength and organization of cortical projections from the retina as well as ocular dominance in the primary visual cortex (V1).[57] The visual cortex is most strongly plastic during early postnatal development; however, our experimental animals were adult cats at approximately 1 year of age. Previous studies have reported rapid reorganization of the cortical retinotopic map in response to retinal insult in the adult feline and macaque; however, this reorganization resulted only from a bilateral loss in vision, and organization was conserved when lesions were formed in only one eye.[58–61] Given that our model had only unilateral visual loss and that we did not examine these changes over time (only at 12 weeks post injection compared to the control baseline), it is unclear whether the effect we observed is a result of similar processes or something different.

Due to the acute (2–3 days) nature of our implantation and stimulation, we could not explore how visual pathway remodeling might influence (or be influenced by) long-term retinal stimulation, but chronic implantation and stimulation of a suprachoroidal array has been previously tested in normally sighted feline[15] and both the impedances and the cortical responses to stimulation were similar in 3-month chronically implanted normally sighted animals to our acutely implanted controls. An interesting next step would be to see whether long-term suprachoroidal simulation in our animal model induces further changes in stimulation threshold or the location of cortical responses.

Finally, our spike window analysis in the cortex was short, and, although we did not observe significant activation of the cortex post 20 ms, previous studies have reported subtle effects at a longer time scale than our analysis reports here.[12] Although we believe our analysis window accounts for the majority of ganglion cell and inner retinal mediated activity,[33] a more thorough analysis of later window activity would be very useful to further tease out the contribution of various surviving or degenerated cell types in the retina. Given that the response latencies triggered by activation of different cell types have significant overlap, perhaps a study involving the application of retinal blockers in degenerated retina in a manner similar to Boinagrov et al.[33] would be the logical next step to further examine retinal contributions independently.

Müller Cell Gliosis in the Retina Correlates to Stimulation Threshold

The suprachoroidal positioning of our retinal array enabled removal of the implanted device without directly affecting retinal integrity, allowing us to compare local histologic variations in the retina with cortical responses to single retinal electrode stimulation. At 12 weeks post ATP injection, abnormal expression of rhodopsin was apparent within the cell bodies of the remaining photoreceptors. Similar abnormal nuclear opsin expression has previously been reported in other models of retinal degeneration.[62,63] Changes in calretinin-labeled amacrine and horizontal cell morphology were also apparent, including the presence of aberrant synapses extending into the outer retina. A thick glial scar was commonly observed across the inner and outer retinas, encapsulating the surviving neural tissue. Retinal ganglion cells appeared well conserved. These features are consistent with mid-to-late stage remodeling events reported in ATP-injected cat and rat retinae[24] and other models of retinal degeneration.[7,64,65]

Investigative Ophthalmology & Visual Science

When local variations in retinal layer thickness, gliosis, and ganglion cell density were correlated with individual electrode thresholds in the implanted degenerate and control retinas, retinal ganglion cell count and GFAP expression were found to correlate with cortical threshold in the ATP-injected eyes. In contrast, only retinal ganglion cell count correlated with threshold in control eyes and there was no correlation with the thickness of the remaining neural layers and cortical threshold in either condition. In our clinical trial in patients with retinitis pigmentosa, and in a similar trial using an epiretinal prosthesis, perceptual thresholds in response to suprachoroidal implant stimulation did not correlate with retinal thickness.[19,66] This further suggests that, in humans and in the current feline model, simple local measurements of retinal integrity such as OCT thickness profiles may not accurately predict the efficacy of an implanted device.

This study provides in vivo confirmation that local variation in retinal ganglion cell density predicts retinal implant efficacy. However, given that retinal ganglion cell density was not significantly different between conditions and the low r^2 value contribution of RGC count to the model suggesting a smaller contribution to threshold change, a loss of retinal ganglion cells cannot be the primary explanation for the higher mean thresholds observed across the ATP-injected eyes. Instead, our results indicate localized regions of Müller cell gliosis could better correlate with factors that lead to higher cortical threshold to retinal stimulation in the degenerated retina. Müller cell gliosis would form a fibrotic, high-density tissue that would increase the resistive properties of the retina in a manner similar to that observed in glial scars that form as a response to chronic electrode implantation in the cortex.[67–69] Additionally, fibrotic tissue may physically increase the distance between an array and functional cell populations. Indeed, in our human trial that measured perceptual thresholds in participants implanted with a suprachoroidal implant, we found distance from the neural retina, but not total retinal thickness, to be a major contributor to perceptual threshold increases over time.[19] Müller cell gliosis is also known to correlate with other markers of retinal remodeling,[8,65] such as bipolar cell atrophy and loss, and morphologic changes such as neuronal shrinkage might also have contributed to elevated thresholds as has been shown in a feline model of the deafened cochleae.[70] Areas with Müller cell gliosis in our model may thus be responding poorly to retinal stimulation primarily due to inner retinal atrophy, while superficially maintaining the appearance of a greater retinal thickness.

The ATP model of retinal degeneration seems to create a severe glial reaction within the inner and outer retina to an extent beyond most classical descriptions of photoreceptor degeneration. An variably thickened inner retinal profile has been reported in many photoreceptor degenerations such as X-linked and rhodopsin mutation retinitis pigmentosa,[71,72] Leber's congenital amaurosis[73] and ABCA4 retinal degeneration.[74] Changes in Müller cell and astrocyte expression leading to gliosis within the inner retina have been examined in several genetic models of retinal degeneration and are thought to be the result of ongoing retinal remodeling.[75,76] Given that a thickened inner retinal profile is most pronounced in rapid forms of retinal degeneration, we think it most likely that a thick inner retinal profile may naturally result from the gliotic reaction to acute photoreceptor death and is not a feature specific to ATP induced phototoxicity. Müller cell gliosis and subsequent inner retinal thickening in our model most closely resembles inner retinal changes reported in Leber's congenital amaurosis, where the total retinal thickness profiles can even increase as a result in early stages of the disease.[73] Given that most patients considered eligible for visual restoration with a suprachoroidal or subretinal retinal prosthesis have late-stage retinitis pigmentosa where the majority of glial reaction has subsided, our specific findings are likely to apply only in full to a small subset of implantable patients with more rapid disease onset. More broadly, our results suggest that local variation in retinal integrity is important to consider when optimizing device efficacy, and simple measurements of laminar thicknesses should be used cautiously to inform, for example, patient selection or device placement as they may not be an indicator of more directly salient changes in the retina such as RGC loss or the presence of a glial scar.

In summary, a single intravitreal injection of ATP induced photoreceptor degeneration and caused changes in neural and glial cell morphology consistent with retinal remodeling in the feline eye. A suprachoroidal stimulating array was able to induce activation of the degenerate retina at 12 weeks post ATP injection, resulting in robust cortical responses. Notably, the target neural population remained capable of initiating and propagating action potentials in response to an electrical stimulus. Higher levels of charges were required to stimulate the ATP-injected eye to induce a threshold cortical response. Retinal ganglion cell density and the extent of retinal gliosis under an electrode, but not thickness of total or outer retina, correlated with increased cortical thresholds in response to retinal stimulation in the ATP-injected eyes. Our data suggest that retinal ganglion cell survival is not the sole contributor to increased cortical thresholds to suprachoroidal stimulation in retinal degeneration. Rather, glial remodeling can also be used to predict the efficacy of suprachoroidal electrical stimulation. These results highlight that for optimal restoration of vision using prostheses, local variations in retinal structure, such as the extent of gliosis, may be important.

Acknowledgments

Supported by the Australian Research Council through its Special Research Initiative in Bionic Vision Science and Technology grant to Bionic Vision Australia and by National Health and Medical Research Council project grants (APP1021042; APP1061419) (ELF) by Retina Australia. The Bionics Institute and Center for Eye Research Australia receive Operational Infrastructure Support from the Victoria Government.

Disclosure: **F.P. Aplin**, None; **E.L. Fletcher**, None; **C.D. Luu**, None; **K.A. Vessey**, None; **P.J. Allen**, None; **R.H. Guymer**, None; **R.K. Shepherd**, None; **M.N. Shivdasani**, None

References

1. Humayun MS, Dorn JD, da Cruz L, et al. Interim results from the international trial of Second Sight's visual prosthesis. *Ophthalmology*. 2012;119:779–788.
2. Stingl K, Bartz-Schmidt KU, Besch D, et al. Artificial vision with wirelessly powered subretinal electronic implant alpha-IMS. *Proc R Soc Lond B Biol Sci*. 2013;280:e20130077.
3. Ayton LN, Blamey PJ, Guymer RH, et al. First-in-human trial of a novel suprachoroidal retinal prosthesis. *PLoS One*. 2014;9:e0115239.
4. Fujikado T, Kamei M, Sakaguchi H, et al. Testing of semichronically implanted retinal prosthesis by suprachoroidal-transretinal stimulation in patients with retinitis pigmentosa. *Invest Ophthalmol Vis Sci*. 2011;52:4726–4733.
5. Chow AY, Chow VY, Packo KH, Pollack JS, Peyman GA, Schuchard R. The artificial silicon retina microchip for the treatment of vision loss from retinitis pigmentosa. *Arch Ophthalmol*. 2004;122:460–469.
6. Rizzo JF, Wyatt J, Loewenstein J, Kelly S, Shire D. Perceptual efficacy of electrical stimulation of human retina with a

microelectrode array during short-term surgical trials. *Invest Ophthalmol Vis Sci*. 2003;44:5362–5369.

7. Marc RE, Jones BW, Watt CB, Strettoi E. Neural remodeling in retinal degeneration. *Prog Retin Eye Res*. 2003;22:607–655.
8. Jones BW, Watt CB, Marc RE. Retinal remodelling. *Clin Exp Optom*. 2005;88:282–291.
9. Dorn JD, Ahuja AK, Caspi A, et al. The detection of motion by blind subjects with the epiretinal 60-electrode (Argus II) retinal prosthesis. *JAMA Ophthalmol*. 2013;131:183–189.
10. Humayun MS, Weiland JD, Fujii GY, et al. Visual perception in a blind subject with a chronic microelectronic retinal prosthesis. *Vision Res*. 2003;43:2573–2581.
11. Zrenner E. Fighting blindness with microelectronics. *Sci Transl Med*. 2013;5:210ps216.
12. Lorach H, Goetz G, Smith R, et al. Photovoltaic restoration of sight with high visual acuity. *Nat Med*. 2015;21:476–482.
13. Shivdasani MN, Fallon JB, Luu CD, et al. Visual cortex responses to single- and simultaneous multiple-electrode stimulation of the retina: implications for retinal prostheses. *Invest Ophthalmol Vis Sci*. 2012;53:6291–6300.
14. Leung RT, Nayagam DA, Williams RA, et al. Safety and efficacy of explanting or replacing suprachoroidal electrode arrays in a feline model. *Clin Exp Ophthalmol*. 2014;3:247–258.
15. Nayagam DA, Williams RA, Allen PJ, et al. Chronic electrical stimulation with a suprachoroidal retinal prosthesis: a preclinical safety and efficacy study. *PLoS One* 2014;9:e97182.
16. John SE, Shivdasani MN, Williams CE, et al. Suprachoroidal electrical stimulation: Effects of stimulus pulse parameters on visual cortical responses. *J Neural Eng*. 2013;10:e056011.
17. Dumm G, Fallon JB, Williams CE, Shivdasani MN. Virtual electrodes by current steering in retinal prostheses. *Invest Ophthalmol Vis Sci*. 2014;55:8077–8085.
18. Cicione R, Shivdasani MN, Fallon JB, et al. Visual cortex responses to suprachoroidal electrical stimulation of the retina: Effects of electrode return configuration. *J Neural Eng*. 2012;9:e036009.
19. Shivdasani MN, Sinclair NC, Dimitrov PN, et al. Factors affecting perceptual thresholds in a suprachoroidal retinal prosthesis. *Invest Ophthalmol Vis Sci*. 2014;55:6467–6481.
20. Nishida K, Kamei M, Kondo M, et al. Efficacy of suprachoroidal-transretinal stimulation in a rabbit model of retinal degeneration. *Invest Ophthalmol Vis Sci*. 2010;51:2263–2268.
21. Chan LH, Ray A, Thomas BB, Humayun MS, Weiland JD. In vivo study of response threshold in retinal degenerate model at different degenerate stages. *Conf Proc IEEE Eng Med Biol Soc*. 2008;1781–1784.
22. Aplin FP, Luu CD, Vessey KA, Guymer RH, Shepherd RK, Fletcher EL. ATP-induced photoreceptor death in a feline model of retinal degeneration. *Invest Ophthalmol Vis Sci*. 2014;55:8319–8329.
23. Aplin FP, Vessey KA, Luu CD, Guymer RH, Shepherd RK, Fletcher EL. Retinal changes in an ATP-induced model of retinal degeneration. *Front Neuroanat*. 2016;10.
24. Vessey KA, Greferath U, Aplin FP, et al. Adenosine triphosphate-induced photoreceptor death and retinal remodeling in rats. *J Comp Neurol*. 2014;522:2928–2950.
25. Puthussery T, Fletcher E. Extracellular ATP induces retinal photoreceptor apoptosis through activation of purinoceptors in rodents. *J Comp Neurol*. 2009;513:430–440.
26. Gekeler F, Szurman P, Grisanti S, et al. Compound subretinal prostheses with extra-ocular parts designed for human trials: successful long-term implantation in pigs. *Graefe's Arch Clin Exp Ophthalmol*. 2007;245:230–241.
27. Güven D, Weiland JD, Fujii G, et al. Long-term stimulation by active epiretinal implants in normal and RCD1 dogs. *J Neural Eng*. 2005;2:S65–S73.
28. Terasawa Y, Tashiro H, Nakano Y, Osawa K, Ozawa M. Safety assessment of semichronic suprachoroidal electrical stimulation to rabbit retina. *Conf Proc IEEE Eng Med Biol Soc*. 2013;3567–3570.
29. Villalobos J, Nayagam DA, Allen PJ, et al. A wide-field suprachoroidal retinal prosthesis is stable and well tolerated following chronic implantation. *Invest Ophthalmol Vis Sci*. 2013;54:3751–3762.
30. Villalobos J, Allen PJ, McCombe MF, et al. Development of a surgical approach for a wide-view suprachoroidal retinal prosthesis: evaluation of implantation trauma. *Graefe's Arch Clin Exp Ophthalmol*. 2012;250:399–407.
31. Fallon JB, Irving S, Pannu SS, et al. Second spatial derivative analysis of cortical surface potentials recorded in cat primary auditory cortex using thin film surface arrays: comparisons with multi-unit data. *J Neurosci Methods*. 2016;267:14–20.
32. Fallon JB, Irvine DR, Shepherd RK. Cochlear implant use following neonatal deafness influences the cochleotopic organization of the primary auditory cortex in cats. *J Comp Neurol*. 2009;512:101–114.
33. Boinagrov D, Pangratz-Fuehrer S, Goetz G, Palanker D. Selectivity of direct and network-mediated stimulation of the retinal ganglion cells with epi-, sub- and intra-retinal electrodes. *J Neural Eng*. 2014;11:026008.
34. Villalobos J, Fallon JB, Nayagam DA, et al. Cortical activation following chronic passive implantation of a wide-field suprachoroidal retinal prosthesis. *J Neural Eng*. 2014;11:046017.
35. Eckhorn R, Wilms M, Schanze T, et al. Visual resolution with retinal implants estimated from recordings in cat visual cortex. *Vision Res*. 2006;46:2675–2690.
36. Elfar SD, Cottaris NP, Iezzi R, Abrams GW. A cortical (V1) neurophysiological recording model for assessing the efficacy of retinal visual prostheses. *J Neurosci Methods*. 2009;180:195–207.
37. Fariss RN, Molday RS, Fisher SK, Matsumoto B. Evidence from normal and degenerating photoreceptors that two outer segment integral membrane proteins have separate transport pathways. *J Comp Neurol*. 1997;387:148–156.
38. Linberg KA, Lewis GP, Shaaw C, Rex TS, Fisher SK. Distribution of S-and M-cones in normal and experimentally detached cat retina. *J Comp Neurol*. 2001;430:343–356.
39. Pasteels B, Rogers J, Blachier F, Pochet R. Calbindin and calretinin localization in retina from different species. *Vis Neurosci*. 1990;5:1–16.
40. MacNeil MA, Purrier S, Rushmore RJ. The composition of the inner nuclear layer of the cat retina. *Vis Neurosci*. 2009;26:365–374.
41. Fyk-Kolodziej B, Dzhagaryan A, Qin P, Pourcho RG. Immunocytochemical localization of three vesicular glutamate transporters in the cat retina. *J Comp Neurol*. 2004;475:518–530.
42. Vessey KA, Fletcher EL. Rod and cone pathway signalling is altered in the P2X7 receptor knock out mouse. *PLoS One*. 2012;7:e29990.
43. Vessey KA, Wilkinson-Berka JL, Fletcher EL. Characterization of retinal function and glial cell response in a mouse model of oxygen-induced retinopathy. *J Comp Neurol*. 2011;519:506–527.
44. Lewis GP, Erickson PA, Kaska DD, Fisher SK. An immunocytochemical comparison of Müller cells and astrocytes in the cat retina. *Exp Eye Res*. 1988;47:839–853.
45. Rodriguez AR, de Sevilla Müller LP, Brecha NC. The RNA binding protein RBPMS is a selective marker of ganglion cells in the mammalian retina. *J Comp Neurol*. 2014;522:1411–1443.
46. Aarts E, Verhage M, Veenvliet JV, Dolan CV, van der Sluis S. A solution to dependency: using multilevel analysis to accommodate nested data. *Nat Neurosci*. 2014;17:491–496.

Investigative Ophthalmology & Visual Science

47. West BT, Welch KB, Galecki AT. Linear Mixed Models: A Practical Guide Using Statistical Software. Boca Raton, FL: CRC Press; 2014.
48. Tassinari G, Bentivoglio M, Chen S, Campara D. Overlapping ipsilateral and contralateral retinal projections to the lateral geniculate nucleus and superior colliculus in the cat: a retrograde triple labelling study. *Brain Res Bull*. 1997;43: 127–139.
49. Illing RB, Wässle H. The retinal projection to the thalamus in the cat: a quantitative investigation and a comparison with the retinotectal pathway. *J Comp Neurol*. 1981;202:265–285.
50. Brummer SB, Turner MJ. Electrochemical considerations for safe electrical stimulation of the nervous system with platinum electrodes. *IEEE Trans Biomed Eng*. 1977;24:59–63.
51. Shannon RV. A model of safe levels for electrical stimulation. *IEEE Trans Biomed Eng*. 1992;39:424–426.
52. Cogan SF. Neural stimulation and recording electrodes. *Annu Rev Biomed Eng*. 2008;10:275–309.
53. Sekirnjak C, Hulse C, Jepson LH, et al. Loss of responses to visual but not electrical stimulation in ganglion cells of rats with severe photoreceptor degeneration. *J Neurophysiol*. 2009;102:3260–3269.
54. O'Hearn TM, Sadda SR, Weiland JD, Maia M, Margalit E, Humayun MS. Electrical stimulation in normal and retinal degeneration (rd1) isolated mouse retina. *Vision Res*. 2006;46: 3198–3204.
55. Siu T, Morley J. Implantation of episcleral electrodes via anterior orbitotomy for stimulation of the retina with induced photoreceptor degeneration: an in vivo feasibility study on a conceptual visual prosthesis. *Acta Neurochirurgica* 2008;150: 477–485.
56. Wässle H, Illing RB. The retinal projection to the superior colliculus in the cat: A quantitative study with HRP. *J Comp Neurol*. 1980;190:333–356.
57. Espinosa JS, Stryker MP. Development and plasticity of the primary visual cortex. *Neuron*. 2012;75:230–249.
58. Kaas JH, Krubitzer LA, Chino YM, Langston AL, Polley EH, Blair N. Reorganization of retinotopic cortical maps in adult mammals after lesions of the retina. *Science*. 1990;248:229.
59. Chino YM, Kaas JH, Smith EL III, Langston AL, Cheng H. Rapid reorganization of cortical maps in adult cats following restricted deafferentation in retina. *Vision Res*. 1992;32:789–796.
60. Gilbert CD, Wiesel TN. Receptive field dynamics in adult primary visual cortex. *Nature*. 1992;356:150–152.
61. Spear PD, Langsetmo A, Smith DC. Age-related changes in effects of monocular deprivation on cat striate cortex neurons. *J Neurophyiol*. 1980:559–580.
62. Gao J, Cheon K, Nusinowitz S, et al. Progressive photoreceptor degeneration, outer segment dysplasia, and rhodopsin mislocalization in mice with targeted disruption of the retinitis pigmentosa–1 (Rp1) gene. *Proc Natl Acad Sci U S A*. 2002;99: 5698–5703.
63. Fletcher EL, Jobling AI, Vessey KA, Luu C, Guymer RH, Baird PN. Animal models of retinal disease. *Prog Mol Biol Transl Sci*. 2011:211–286.
64. Jones BW, Watt CB, Frederick JM, et al. Retinal remodeling triggered by photoreceptor degenerations. *J Comp Neurol*. 2003;464:1–16.
65. Marc RE, Jones BW, Watt CB, Vazquez-Chona F, Vaughan DK, Organisciak DT. Extreme retinal remodeling triggered by light damage: Implications for age related macular degeneration. *Mol Vis*. 2008;14:782–806.
66. de Balthasar C, Patel S, Roy A, et al. Factors affecting perceptual thresholds in epiretinal prostheses. *Invest Ophthalmol Vis Sci*. 2008;49:2303.
67. Harris JP, Tyler DJ. Biological mechanical, and technological considerations affecting the longevity of intracortical electrode recordings. *Crit Rev Biomed Eng*. 2014;41:435–456.
68. Griffith RW, Humphrey DR. Long-term gliosis around chronically implanted platinum electrodes in the Rhesus macaque motor cortex. *Neurosci Lett*. 2006;406:81–86.
69. Polikov VS, Tresco PA, Reichert WM. Response of brain tissue to chronically implanted neural electrodes. *J Neurosci Methods*. 2005;148:1–18.
70. Shepherd RK, Javel E. Electrical stimulation of the auditory nerve. I. Correlation of physiological responses with cochlear status. *Hear Res*. 1997;108:112–144.
71. Aleman TS, Cideciyan AV, Sumaroka A, et al. Retinal laminar architecture in human retinitis pigmentosa caused by rhodopsin gene mutations. *Invest Ophthalmol Vis Sci*. 2008;49:1580–1590.
72. Aleman TS, Cideciyan AV, Sumaroka A, et al. Inner retinal abnormalities in X-linked retinitis pigmentosa with RPGR mutations. *Invest Ophthalmol Vis Sci*. 2007;48:4759–4765.
73. Jacobson SG, Cideciyan AV, Aleman TS, et al. RDH12 and RPE65, Visual cycle genes causing Leber congenital amaurosis, differ in disease expression. *Invest Ophthalmol Vis Sci*. 2007; 48:332–338.
74. Huang WC, Cideciyan AV, Roman AJ, et al. Inner and outer retinal changes in retinal degenerations associated with ABCA4 mutations retinal remodeling in ABCA4 disease. *Invest Ophthalmol Vis Sci*. 2014;55:1810–1822.
75. Fernández-Sánchez L, Lax P, Campello L, Pinilla I, Cuenca N. Astrocytes and Müller cells changes during retinal degeneration in a transgenic rat model of retinitis pigmentosa. *Front Cell Neurosci*. 2015;9:484.
76. Roesch K, Stadler MB, Cepko CL. Gene expression changes within Müller glial cells in retinitis pigmentosa. *Mol Vis*. 2012; 18:1197–1214.

Investigative Ophthalmology & Visual Science